Equilibrium Configurations for a Territorial Model[*]

Ronald Votel[†], David A. W. Barton[‡], Takahide Gotou[§], Takeshi Hatanaka[§], Masayuki Fujita[§], and Jeff Moehlis[¶]

Abstract. We consider a territorial model based on Voronoi tessellations, which form a partition of a planar region by enclosing each agent in a polygon such that every point within the polygon is closest to that agent instead of any other. Equilibria for this model correspond to centroidal Voronoi tessellations. For rectangular domains and for small population sizes, we show that there can be distinct coexisting stable equilibrium configurations, including the possibility of stable equilibria that are not related by symmetry. By considering randomly distributed initial positions, we give a statistical characterization of the basins of attraction for these equilibria in the case of a square domain. Furthermore, we show that the final territory that an agent occupies can have a wide range of sizes, which suggests that an individual can obtain a competitive advantage or disadvantage due entirely to its initial position. By treating the ratio of the length of the shorter side to the length of the longer side of the rectangle as a bifurcation parameter, we also numerically explore how stable and unstable equilibrium configurations are related to each other. Results for three agents are verified through experiments using robots which move according to a related territorial algorithm.

Key words. territorial behavior, Voronoi tessellations, symmetry

AMS subject classifications. 37G35, 37G40, 37N25

DOI. 10.1137/070710123

1. Introduction. One of the most fundamental problems in all of biology is to understand how organisms divide space into discrete territories that define their abilities to capture vital resources and access mates. A *territory* is a geographical area that an individual animal consistently defends against other individuals from its own species, typically in an attempt to maximize its reproductive opportunities and/or to secure food resources for itself and its young [37]. Territoriality is common across nearly all major groups of organisms on the planet. While higher animals like vertebrates exhibit the most obvious territorial boundaries, lower animals like invertebrates, plants, fungi, and possibly even bacteria are known to aggressively

defend space through behaviors and chemicals.

We highlight the experiment in [2], which involved placing a number of mouthbreeder fish *Tilapia mossambica* in a rectangular pool with a sandy floor. The males vying for suitable breeding territory dug pits, spitting sand away from their pit centers. The resulting rims of the pits were visualized in a top-view photograph taken with a polarizing filter, which showed that the final arrangement of pits resembled a honeycomb-like pattern consisting mainly of pentagonal and hexagonal regions. It has been shown [24, 36] that these territories can be approximated by Voronoi tessellations [15], a partition of the (top-view projection of the) pool formed by enclosing each fish in a polygon such that every point within the polygon is closest to that particular fish instead of any other. Other observational determinations of territorial boundaries include [19, 3, 4, 5, 14].

Various mathematical models have been developed to understand sizes and/or shapes that territories will take for different species of animals. Some models determine the optimal size for an agent's territory based on a balance between the benefits of having a larger territory with the costs of defending such a territory; see [1] and references therein. However, such models often assume that the agents can adjust the boundaries of their territories without consideration of the boundaries of their neighbors' boundaries [1, 33]. Attempts to explicitly account for interactions between neighboring agents have included partial differential equation models describing the response of agents to boundary scent marks [28, 32], models in which agents associate an attractiveness to different spatial regions based on their prior interactions between other agents in each region [35], and game theoretic approaches [30, 34, 33].

In this paper, we consider an alternative model for territorial behavior based on Voronoi tessellations which captures interactions between agents in a simple way [36]; also see [22, 23, 15]. Here, at a given time and for each agent, we calculate the set of points in the domain of interest which is closer to that agent than to any other. Such a partition of the domain is called a Voronoi tessellation, and the set of such points for each agent is called the agent's Voronoi cell. The agents then move toward the centroid of their current Voronoi cell, continuing such adjustment until an equilibrium state is reached. An agent's Voronoi cell at such an equilibrium is considered to be its territory. We note that these equilibria are centroidal Voronoi tessellations, that is, Voronoi tessellations for which the generators of the Voronoi cells are the centroids of the cells defined using a constant density function [15]. This model captures the tendency of each agent to occupy territory so that it is as far from others as possible, and the notion that aggression of an agent decreases monotonically with distance from the center of its territory. It ignores environmental influences and heterogeneity in the individuals' characteristics or behavior and assumes that the settlement is synchronous, i.e., that all agents begin competing for territory at the same time. The simulations in [36] of this model focused on the behavior of large numbers of agents ($N = 500$) for periodic boundary conditions and showed good agreement between the statistics of the territorial shapes from the model and those found for the experiment in [2]. We remark that related models based on Voronoi tessellations have become popular in the robotics literature, e.g., [9, 26, 20]. Here the motivation might be the performance of spatially distributed sensing tasks such as surveillance or search and rescue.

In section 2 we describe the model from [36] in more detail. In section 3 we discuss stability properties for equilibrium configurations. In section 4 we consider the model for

a small population ($N = 2$ up to $N = 9$) in a square domain for which the boundaries of the domain form boundaries of the Voronoi cells as appropriate. We find that for certain population sizes there are distinct coexisting stable equilibrium configurations, sometimes related by symmetry and sometimes not. An agent can end up with a much larger or smaller territory (and corresponding competitive advantage or disadvantage) due entirely to the initial positions of the agents, and we give a statistical characterization of the likelihood of the system reaching different equilibria. In section 5, we consider the model for a small population in a rectangular domain, again with the boundaries of the domain forming boundaries of the Voronoi cells as appropriate. By treating L, the ratio of the length of the shorter side to the length of the longer side of the rectangle, as a bifurcation parameter, we numerically explore how stable and unstable equilibrium configurations are related to each other and identify rectangles which have coexisting stable equilibrium configurations. Results for three agents are verified through experiments using robots which move according to a related territorial algorithm, as described in section 6. Concluding remarks are given in section 7. We remark that we focus on small numbers of agents and square and rectangular domain shapes because these are natural for controlled laboratory experimentation.

2. The model. We consider N agents in a two-dimensional rectangular domain D with sides of length 1 and L. Without loss of generality, we take $L \leq 1$, where equality corresponds to the special case of a square domain. The location of the ith agent at time step n is $\mathbf{x}_i^{(n)}$. The Voronoi cell [15] for the ith agent at time step n is defined as

$$(2.1) \qquad V_i^{(n)} = \{\mathbf{x} \in D \mid |\mathbf{x} - \mathbf{x}_i| < |\mathbf{x} - \mathbf{x}_j| \qquad \text{for } j = 1, \ldots, N, \ j \neq i\},$$

with centroid

$$(2.2) \qquad \mathbf{c}_i^{(n)} = \frac{1}{|V_i^{(n)}|} \int_{V_i^{(n)}} \mathbf{x} d\mathbf{x},$$

where $|V_i^{(n)}|$ is the area of Voronoi cell $V_i^{(n)}$. Each agent's location at time step $n + 1$ is determined as [36]

$$(2.3) \qquad \mathbf{x}_i^{(n+1)} = \mathbf{x}_i^{(n)} + \left(\mathbf{c}_i^{(n)} - \mathbf{x}_i^{(n)}\right)/M, \qquad i = 1, \ldots, N,$$

where M is a constant greater than or equal to 1; that is, each agent moves a fraction of the distance toward the centroid of its Voronoi cell. Biologically, M measures the extent to which an agent moves toward the centroid of its Voronoi cell before reevaluating how to move. We remark that the centroids $\mathbf{c}_i$ are nonlinear functions of the locations of the agents; such nonlinearity leads to the richness of the results reported below.

We simulate this model using MATLAB, taking advantage of its built-in `voronoi` and `voronoin` commands, and using John Burkhardt's publicly available MATLAB geometry command package to perform certain calculations such as finding centroids of the Voronoi cells from their vertices [7]. To force the boundaries of Voronoi cells to be the boundaries of D, as appropriate, we place four images of each agent outside D (one reflected about each side of D) for each agent.

Numerical simulation reveals that for all cases considered ($N = 2, \ldots, 9$, various values of M, and many random and nonrandom initial conditions) the dynamical system (2.3) equilibrates as $n \to \infty$ to a stable equilibrium configuration satisfying

$$(2.4) \qquad\qquad \mathbf{x}_i^{(n+1)} = \mathbf{x}_i^{(n)}, \qquad i = 1, \ldots, N.$$

We find that for certain values of N and L, there are distinct coexisting stable equilibrium configurations, sometimes related by symmetry and sometimes not. For this model, we do not find more complicated attractors such as periodic orbits.

3. Stability properties of equilibrium configurations. The stability properties of the equilibrium configurations may be determined numerically by calculating the eigenvalues (using finite differences) of the linearization of the system about the equilibrium configuration. The following results show that the existence and stability properties of equilibrium configurations are independent of the parameter M.

Proposition 3.1. The same equilibrium configurations exist for any value of M.

Proof. The locations of the centroids of Voronoi cells are independent of M, so if the system is at an equilibrium configuration for a particular value of M, meaning that all agents are at the centroids of their Voronoi cells, then it will also be an equilibrium configuration for any other value of M. ∎

We now give several results which show that the stability properties of the equilibrium configurations for any M can be determined by the stability properties for $M = 1$.

Proposition 3.2. If an equilibrium configuration is asymptotically stable for $M = 1$, then it is asymptotically stable for all $M > 1$.

Proof. Since the centroids $\mathbf{c}_i$ are independent of M, the Jacobian of the update map (2.3) evaluated at the equilibrium must take the form

$$(3.1) \qquad\qquad J = I + \frac{K}{M},$$

where I is the $2N \times 2N$ identity matrix, and K is a $2N \times 2N$ matrix which is independent of M. Letting

$$\lambda = 1 + \frac{\mu}{M}$$

be an eigenvalue of J, we see that

$$\det\left[I + \frac{K}{M} - \left(1 + \frac{\mu}{M}\right)I\right] = 0.$$

Simplifying,

$$\det\left[\frac{K}{M} - \frac{\mu}{M}I\right] = 0 \qquad \Rightarrow \qquad \det[K - \mu I] = 0.$$

Thus, μ is an eigenvalue of K, so that μ is independent of M.

Now, if the equilibrium is stable for $M = 1$, then for all eigenvalues

$$(1 + \mu_r)^2 + \mu_i^2 < 1 \qquad \Rightarrow \qquad \mu_i^2 < 1 - (1 + \mu_r)^2,$$

where $\mu = \mu_r + i\mu_i$. Thus,

$$|\lambda|^2 = \left|1 + \frac{\mu}{M}\right|^2 = \left(1 + \frac{\mu_r}{M}\right)^2 + \left(\frac{\mu_i}{M}\right)^2$$

$$(3.2) \qquad < \left(1 + \frac{\mu_r}{M}\right)^2 + \frac{1}{M^2}\left[1 - (1 + \mu_r)^2\right] = 1 + \frac{2\mu_r}{M}\left(1 - \frac{1}{M}\right).$$

Now, since the equilibrium is stable for $M = 1$, we must have

$$-1 < 1 + \mu_r < 1 \qquad \Rightarrow \qquad -2 < \mu_r < 0.$$

Furthermore, for $M > 1$, we have $1 - \frac{1}{M} > 0$. Thus,

$$\frac{2\mu_r}{M}\left(1 - \frac{1}{M}\right) < 0,$$

so from (3.2)

$$|\lambda|^2 < 1.$$

That is, for $M > 1$ all eigenvalues of the Jacobian evaluated at the equilibrium lie within the unit circle so that the equilibrium is asymptotically stable. ∎

We remark that, following [15], one can define the "energy" of a configuration as

$$(3.3) \qquad G = \sum_{i=1}^{N} \int_{\mathbf{x} \in V_i} |\mathbf{x} - \mathbf{x}_i|^2 d\mathbf{x} \equiv \sum_{i=1}^{N} G_i.$$

Notice that G does not depend on M. Applying Proposition 6.2 of [15] in componentwise form, we have

$$(3.4) \qquad \mathbf{x}_i^{(n+1)} = \mathbf{x}_i^{(n)} - \frac{1}{2M|V_i^{(n)}|}\frac{\partial G}{\partial \mathbf{x}_i}.$$

We note that $\mathbf{x}_i^{(n+1)} = \mathbf{x}_i^{(n)}$ for all i (that is, the system is at an equilibrium) if and only if $\frac{\partial G}{\partial \mathbf{x}_i} = 0$ for all i. Now, defining

$$G^{(n)} = G\left(\mathbf{x}_1^{(n)}, \mathbf{x}_2^{(n)}, \ldots, \mathbf{x}_N^{(n)}\right),$$

we have

$$G^{(n+1)} = G\left(\mathbf{x}_1^{(n+1)}, \mathbf{x}_2^{(n+1)}, \ldots, \mathbf{x}_N^{(n+1)}\right)$$

$$= G\left(\mathbf{x}_1^{(n)} - \frac{1}{2M|V_1^{(n)}|}\frac{\partial G}{\partial \mathbf{x}_1}, \mathbf{x}_2^{(n)} - \frac{1}{2M|V_2^{(n)}|}\frac{\partial G}{\partial \mathbf{x}_2}, \ldots, \mathbf{x}_N^{(n)} - \frac{1}{2M|V_N^{(n)}|}\frac{\partial G}{\partial \mathbf{x}_N}\right).$$

Sufficiently close to an equilibrium, we can approximate this as

$$(3.5) \qquad G^{(n+1)} \approx G^{(n)} - \frac{1}{2M}\sum_{i=1}^{N}\frac{1}{|V_i^{(n)}|}\left|\frac{\partial G}{\partial \mathbf{x}_i}\right|^2,$$

where the derivatives are evaluated at $(\mathbf{x}_1^{(n)}, \mathbf{x}_2^{(n)}, \ldots, \mathbf{x}_N^{(n)})$. Thus in a neighborhood of an equilibrium,

$$(3.6) \qquad\qquad\qquad\qquad G^{(n+1)} \leq G^{(n)},$$

with equality only at the equilibrium. We remark that stable equilibria correspond to local minima of G; however, they need not be global minima, as evidenced by the coexisting stable equilibria described below which generically have different values of G. Furthermore, for $M = 1$, Lemma 2.2 of [16] gives an alternative argument which shows that (3.6) *always* holds, with equality only when the system is at an equilibrium.

Proposition 3.3. *If an equilibrium configuration is unstable for $M = 1$, then it is unstable for all $M > 1$.*

Proof. Suppose that the equilibrium $\mathbf{X}$ is unstable for $M = 1$. Writing the update map (2.3) as $\mathbf{x}^{(n+1)} = \mathbf{f}(\mathbf{x}^{(n)})$, the unstable manifold of $\mathbf{X}$ is the set

$$W^u(\mathbf{X}) = \{\mathbf{x} \mid \mathbf{f}^k(\mathbf{x}) \to \mathbf{X}, k \to -\infty\},$$

that is, the set of points whose infinite iterated sequence of preimages approaches the equilibrium $\mathbf{X}$. Consider a point $\mathbf{X}_u \neq \mathbf{X}$ on $W^u(\mathbf{X})$, sufficiently close to the equilibrium so that (3.5) holds. From (3.6), $G(\mathbf{X}_u) < G(\mathbf{f}^{-1}(\mathbf{X}_u)) < G(\mathbf{f}^{-2}(\mathbf{X}_u)) < \ldots$. Thus, $G(\mathbf{X}_u) < G(\mathbf{X})$; we remark that this relationship holds for all $M > 1$ since G is independent of M.

Since $\mathbf{X}_u$ is not an equilibrium, $G(\mathbf{f}(\mathbf{X}_u)) < G(\mathbf{X}_u) < G(\mathbf{X})$, so (3.5) with $M = 1$ implies that

$$\sum_{i=1}^{N} \frac{1}{|V_i^{(n)}|} \left| \frac{\partial G}{\partial \mathbf{x}_i} \right|^2 > 0,$$

where the derivatives are evaluated at $\mathbf{X}_u$. But then, for the initial state $\mathbf{X}_u$, (3.5) implies for *any* $M > 1$ that G will decrease upon iteration of the update map, giving a value of G smaller than that at the equilibrium. Upon further iteration G will continue to decrease, so that the trajectory cannot approach the equilibrium.

We remark that it is not possible that a single iteration could take a point outside of the region of validity of (3.5) directly to the equilibrium: at the equilibrium the agents are at the centroids of their Voronoi cells, and for $M > 1$ an iteration moves each agent only a *fraction* of the distance toward the centroid of its Voronoi cell.

Thus, the equilibrium must also be unstable for $M > 1$. ∎

We note that if the eigenvalues of the Jacobian are always real and positive for $M = 1$, then an unstable equilibrium must have at least one eigenvalue $\lambda = 1 + \mu_r > 1$. For this eigenvalue $\mu_r > 0$, so $1 + \frac{\mu_r}{M} > 1$ for $M > 1$; that is, the equilibrium is also unstable for $M > 1$. For all equilibrium configurations described below, we find numerically that the eigenvalues are real and positive for $M = 1$, so this simpler proof of Proposition 3.3 holds. We are unaware of a rigorous argument that the eigenvalues must always be real and positive, although (3.4) implies that the Jacobian will be symmetric, and hence that the eigenvalues will be real, when the equilibrium configuration has the same value of $|V_i|$ for $i = 1, \ldots, N$.

Putting together Propositions 3.1, 3.2, and 3.3, we conclude that if we want to determine the existence and stability properties of equilibrium configurations for our model, we can just consider the case $M = 1$.

4. Results for square container.

4.1. Symmetry considerations. Before giving details of the stable equilibrium configurations, it is helpful to clarify the symmetry aspects of this system by using a treatment based on [17, 8, 18, 25, 31]. (Also see [29] for a nice introduction to group theory.) When D is a square, the evolution equations (2.3) are equivariant with respect to the eight element group D_4, which is generated by a $90°$ rotation R (which we take to be counterclockwise) and a diagonal reflection d (which we take to be about the line from the lower left to the upper right corner of D). This implies that if X is an equilibrium configuration, then so is every configuration on its group orbit, that is, the set of configurations $\gamma \cdot X$ for all $\gamma \in D_4$, which we denote by $D_4 \cdot X$. The symmetry of an equilibrium configuration X is characterized by its isotropy subgroup

$$(4.1) \qquad \Sigma_X = \{\gamma \in D_4 : \gamma \cdot X = X\},$$

that is, the set of all elements of D_4 which leave X unchanged. In determining the isotropy subgroup and the group orbit, we consider only the shape of the boundaries of the Voronoi cells and in particular do not consider the "labels" for the agents. (This is equivalent to associating all configurations related by the permutation symmetry which relabels agents.) From Proposition 1.2 of [17], we expect that

$$(4.2) \qquad 8 = |D_4| = |\Sigma_X| |D_4 \cdot X|,$$

that is, the number of elements of the group D_4 (namely, 8) equals the product of the size of the isotropy subgoup of X times the number of (distinct) elements in the group orbit of X. Finally, we note that the isotropy subgroups of X and $\gamma \cdot X$ are related by the conjugacy [17]

$$(4.3) \qquad \Sigma_{\gamma \cdot X} = \gamma \Sigma_X \gamma^{-1}.$$

We will use the convention that the order of group element operation is from right to left. For example, in determining the effect of dR on a configuration X (i.e., $dR \cdot X$), we first rotate (R) and then reflect (d). Furthermore, we denote the identity group operation, which leaves the configuration unchanged, by I.

We now illustrate these symmetry ideas for the stable equilibrium configurations found for $N = 3$. Figure 1 shows a configuration X and its group orbit under D_4. Remembering that we consider only the shape of the boundaries of the Voronoi cells in determining the isotropy subgroup, we see that

$$(4.4) \qquad \Sigma_X = \{I, dR\}$$

and that the group orbit of X can be taken to be the set of configurations

$$(4.5) \qquad \{X, R \cdot X, R^2 \cdot X, R^3 \cdot X\}.$$

This is consistent with (4.2). Figure 2 shows the group orbit of the configuration $Y = R \cdot X$. We see that its isotropy subgroup is

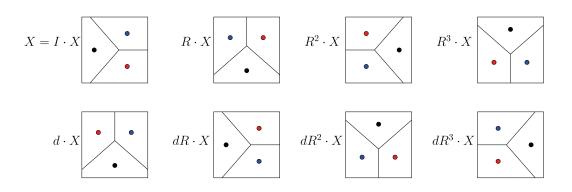$$(4.6) \qquad \Sigma_Y = \{I, dR^3\}.$$

Figure 1. *Sketches of possible stable equilibrium configurations for $N = 3$ agents for a square domain, obtained through the actions of the elements of D_4 on the configuration X. R gives a counterclockwise rotation through $90°$, and d gives a reflection about the diagonal from the lower left to the upper right corners of the square. The color of the agents enables them to be uniquely identified after each group operation. However, in determining the isotropy subgroup of such configurations, we consider only the shapes of boundaries of the Voronoi cells, indicated by lines, and not permutations of the individual agents. We see that this example configuration X has an isotropy subgroup $\Sigma_X = \{I, dR\}$. Furthermore, the group orbit (indicating only distinct configurations based on the boundaries of the Voronoi cells) can be taken to be the set of configurations $\{X, R \cdot X, R^2 \cdot X, R^3 \cdot X\}$.*
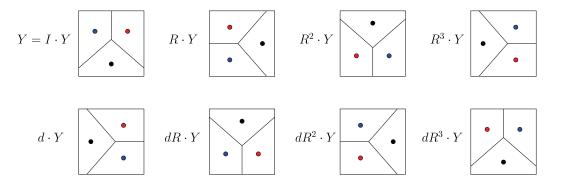

Figure 2. *Sketches of possible stable equilibrium configurations for $N = 3$ agents for a square domain obtained through the actions of the elements of D_4 on the configuration $Y = R \cdot X$. Configuration Y thus has isotropy subgroup $\Sigma_Y = \{I, dR^3\}$. Furthermore, the group orbit can be taken to be the set of configurations $\{Y, R \cdot Y, R^2 \cdot Y, R^3 \cdot Y\}$.*

Now,

$$(4.7) \qquad R \cdot \Sigma_X \cdot R^{-1} = R \cdot \{I, dR\} \cdot R^{-1} = \{I, dR^3\} = \Sigma_{R \cdot X} = \Sigma_Y,$$

as expected from (4.3).

Configurations related by symmetry do not necessarily have different isotropy subgroups. For example, the configurations X and $Y = R \cdot X$ in Figure 3 both have isotropy subgroup

$$\Sigma_X = \Sigma_Y = \{I, R^2, dR, dR^3\}.$$

Note that it is readily shown that $R \cdot \Sigma_X \cdot R^{-1} = \Sigma_X$.
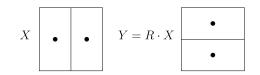
Figure 3. *Stable equilibrium configurations for $N = 2$ agents for a square domain. These configurations are related by symmetry and have the same isotropy subgroup. Recall that we associate configurations related by the permutation symmetry which relabels agents.*
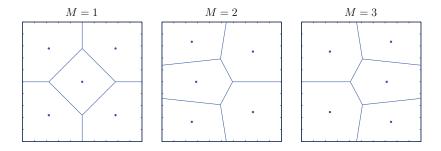

Figure 4. *Equilibrium configurations reached upon iteration of (2.3) for the initial conditions $\mathbf{x}_1 = (0.11, 0.1), \mathbf{x}_j = (0.1, 0.1j), \ j = 2, \ldots, 5$ with M values as labeled, where $D = [0, 1] \times [0, 1]$. See the associated movie files (71012_01.mpg [1.5MB], 71012_02.mpg [1.6MB], and 71012_03.mpg [2.0MB]).*

4.2. Equilibrium configurations. Figure 5 shows one representative from each distinct set of symmetry-related stable equilibria for $N = 2, \ldots, 9$. We find that for $N = 5, 6, 7$, and 9, coexisting stable equilibria which are *not* related by symmetry occur. (Note that for rectangular domains, coexisting stable equilibria not related by symmetry can also exist for $N = 3$ and $N = 4$, as described in section 5.)

The equilibrium configuration that the system settles to for a given set of initial positions depends on M, as illustrated in Figure 4. This motivates the following statistical characterization of the relative sizes of the basins of attraction for the various stable equilibrium configurations. Specifically, Table 1 shows the computed probability of reaching a stable equilibrium configuration of each type with random initial positions distributed uniformly on D for $N = 2, \ldots, 9$ and several values of M. For example, for $N = 5$ and $M = 1$, there is an 86.4% chance of asymptotically approaching one of the elements of the group orbit of the equilibrium configuration Va shown in Figure 5. (Our numerics confirm, within numerical accuracy, the expected result that there is an equal probability of reaching each of the equilibria on a group orbit.) We see that the probability of reaching a particular equilibrium depends at most only weakly on M.

Table 2 gives the areas of the different cells for the configurations shown in Figure 5. We notice that these areas can differ widely for certain N values. For example, when $N = 5$ an agent in cell V_1 (or V_5) for configuration Va occupies 23.8% of the available territory, while an agent in cell V_5 for configuration Vb occupies only 15.6%. More substantially, when $N = 6$ an agent in cell V_1 for configuration VIc occupies 23.3% of the available territory, while an agent in cell V_4 for the same configuration, or an agent in cell V_2 for configuration VIa, occupies only approximately 13%. This suggests that an individual can have a major competitive advantage

Table 1

For the equilibrium configurations for a square domain as labeled in Figure 5, we give the isotropy subgroup and probability of reaching one of the equilibria on its group orbit for random initial positions distributed uniformly on D and different values of M. The probabilities were calculated from 1000 random initial positions for each value of N.

Equil	Isotropy	$M = 1$	$M = 4$	$M = 8$	$M = 12$	$M = 16$	$M = 20$
II	$\{I, R^2, dR, dR^3\}$	100	100	100	100	100	100
III	$\{I, dR\}$	100	100	100	100	100	100
IV	D_4	100	100	100	100	100	100
Va	$\{I, dR\}$	86.4	87.1	88	85.1	85.3	87.5
Vb	D_4	13.6	12.9	12	14.9	14.7	12.5
VIa	$\{I, dR^3\}$	42.4	46.6	46.5	46.6	47.1	46.2
VIb	$\{I, dR^3\}$	20.7	19.6	21.7	20.1	17.1	17.1
VIc	$\{I, d\}$	36.9	33.8	31.8	33.3	35.8	36.7
VIIa	$\{I, dR^2\}$	43.9	44.9	44.6	47.1	47.8	45.4
VIIb	$\{I, dR^3\}$	29.2	30.5	32.2	28.3	27.1	28
VIIc	$\{I, R^2, dR, dR^3\}$	26.9	24.6	23.2	24.6	25.1	26.6
VIII	D_4	100	100	100	100	100	100
IXa	$\{I, dR^3\}$	11.2	12.3	11.3	12.8	12.7	12.4
IXb	D_4	88.8	87.7	88.7	87.2	87.3	87.6

or disadvantage based on territorial size due entirely to the initial positions of the agents, as this determines the configuration which the population equilibrates to and the cell in which each agent ends up.

Similarly, Table 3 gives the energies G_i associated with each Voronoi cell for each stable equilibria, plus the total energy G for the equilibria. This leads to several interesting observations. First, one does not typically find equipartition of energy amongst the Voronoi cells, except for the symmetric configurations II, IV, and IXb; this is seen most extremely for VIc, in which $G_1 = 0.0089$ and $G_4 = 0.0029$. This is presumably because we are considering relatively small N; [15] suggests that equipartitioning of energy will occur for sufficiently large N. Second, the energies of coexisting stable equilibria can be quite similar, in particular for $N = 5, 6, 7$. Recalling results from Table 1 on the differences in the probability of reaching each equilibrium for random initial positions, this suggests that energy alone is not a strong indicator of the relative likelihoods of ending up in different equilibrium states.

While our paper focuses on relatively small numbers of agents, we do find that the number of distinct stable equilibrium configurations grows rapidly with N; see Figure 6, which does not multiply count configurations related by symmetry. We note that many of the stable equilibrium configurations for large N look very similar. While we do not consider the statistical properties of these configurations (e.g., statistics of the areas of the cells, statistics of the number of cells with a given number of edges, etc.) as [36] did for a domain with periodic boundary conditions, we expect that that such statistics would approach those in [36] as N becomes large and the relative number of agents whose cells include part of the boundary of D becomes smaller.

There are also various unstable configurations for a square domain that cannot be found by numerical simulation alone, as will be shown in the next section.
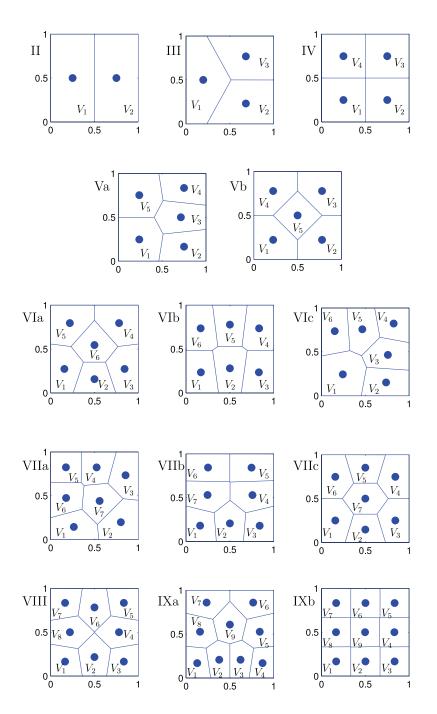
Figure 5. *Stable equilibrium configurations found numerically for $N = 2, \ldots, 9$ for a square domain. Symmetry-related equilibria (i.e., other elements on the group orbit of an equilibrium) are not shown. The equilibria are labeled with a roman numeral indicating the value of N and a lower-case letter to distinguish different equilibria for a given N, if necessary. The index i in the cell label V_i is only for reporting the areas in Table 2; recall that we associate all configurations related by the permutation symmetry which relabels agents.*

Table 2
For the equilibrium configurations for a square domain as labeled in Figure 5, we give the area $|V_i|$ for each Voronoi cell V_i.

Equil	Areas
II	$|V_1| = |V_2| = 0.5$
III	$|V_1| = 0.376 \qquad |V_2| = 0.312 \qquad |V_3| = 0.312$
IV	$|V_1| = |V_2| = |V_3| = |V_4| = 0.25$
Va	$|V_1| = |V_5| = 0.238 \qquad |V_2| = |V_4| = 0.172 \qquad |V_3| = 0.181$
Vb	$|V_1| = |V_2| = |V_3| = |V_4| = 0.211 \qquad |V_5| = 0.156$
VIa	$|V_1| = |V_3| = 0.168 \qquad |V_2| = 0.130$ $|V_4| = |V_5| = 0.192 \qquad |V_6| = 0.150$
VIb	$|V_1| = |V_3| = 0.163 \qquad |V_2| = 0.174$ $|V_4| = |V_6| = 0.171 \qquad |V_5| = 0.158$
VIc	$|V_1| = 0.233 \qquad |V_2| = |V_6| = 0.159$ $|V_3| = |V_5| = 0.158 \qquad |V_4| = 0.131$
VIIa	$|V_1| = |V_3| = 0.154 \qquad |V_2| = 0.172 \qquad |V_4| = |V_6| = 0.129$ $|V_5| = 0.122 \qquad |V_7| = 0.139$
VIIb	$|V_1| = |V_3| = 0.121 \qquad |V_2| = 0.135$ $|V_4| = |V_7| = 0.154 \qquad |V_5| = |V_6| = 0.156$
VIIc	$|V_1| = |V_3| = |V_4| = |V_6| = 0.156$ $|V_2| = |V_5| = 0.118 \qquad |V_7| = 0.139$
VIII	$|V_1| = |V_3| = |V_5| = |V_7| = 0.113 \qquad |V_2| = |V_4| = |V_6| = |V_8| = 0.136$
IXa	$|V_1| = |V_4| = 0.089 \qquad |V_2| = |V_3| = 0.099 \qquad |V_5| = |V_8| = 0.114$ $|V_6| = |V_7| = 0.134 \qquad |V_9| = 0.125$
IXb	$|V_1| = |V_2| = |V_3| = |V_4| = |V_5| = |V_6| = |V_7| = |V_8| = |V_9| = 0.111$

5. Results for rectangular container.

5.1. Symmetry considerations. When D is a (nonsquare) rectangle, the evolution equations (2.3) are equivariant with respect to the four element group

$$\mathrm{D}_2 = \{I, R^2, dR, dR^3\},$$

which is a subgroup of the group D_4 discussed in section 4. The elements R^2, dR, and dR^3 correspond to a rotation by 180°, reflection about the horizontal midplane, and reflection about the vertical midplane, respectively. The possible isotropy subgroups of equilibrium configurations for a rectangular container are D_2, $\{I, R^2\} \cong Z_2$, $\{I, dR\} \cong Z_2$, $\{I, dR^3\} \cong Z_2$, and $\{I\}$. As in section 4, in determining the isotropy subgroup of a configuration we consider only the shape of the boundaries of the Voronoi cells.

5.2. Bifurcation analysis. In order to understand and summarize the existence and stability properties of equilibrium states for the more general rectangular domain and to identify how the different equilibria are related or "connected" to each other, we perform a bifurcation analysis of the territorial model. Specifically, we treat L, the ratio of the length of the shorter side to the length of the longer side of the rectangle, as a bifurcation parameter. Without loss of generality, we take $L \leq 1$, where equality corresponds to the special, degenerate case of a square domain. Note that the bifurcation results are independent of M, which determines the fraction of the distance an agent moves toward the centroid of its Voronoi cell.

Table 3
For the equilibrium configurations for a square domain as labeled in Figure 5, we give the energies G_i associated with each Voronoi cell, and the total energy G. We remark that the sum of the numbers in the second column might not equal the number in the third column due to round-off.

Equil	G_i	$G = \sum_{i=1}^{N} G_i$
II	$G_1 = G_2 = 0.0521$	0.1042
III	$G_1 = 0.0311 \qquad G_2 = G_3 = 0.0175$	0.0662
IV	$G_1 = G_2 = G_3 = G_4 = 0.0104$	0.0417
Va	$G_1 = G_5 = 0.0093 \qquad G_2 = G_4 = 0.0054 \qquad G_3 = 0.0061$	0.0355
Vb	$G_1 = G_2 = G_3 = G_4 = 0.0078 \qquad G_5 = 0.0040$	0.0353
VIa	$G_1 = G_3 = 0.0052 \qquad G_2 = 0.0029$ $G_4 = G_5 = 0.0065 \qquad G_6 = 0.0037$	0.0300
VIb	$G_1 = G_3 = 0.0048 \qquad G_2 = 0.0055$ $G_4 = G_6 = 0.0053 \qquad G_5 = 0.0044$	0.0301
VIc	$G_1 = 0.0089 \qquad G_2 = G_6 = 0.0048$ $G_3 = G_5 = 0.0045 \qquad G_4 = 0.0029$	0.0305
VIIa	$G_1 = G_3 = 0.0045 \qquad G_2 = 0.0053 \qquad G_4 = G_6 = 0.0028$ $G_5 = 0.0025 \qquad G_7 = 0.0032$	0.0256
VIIb	$G_1 = G_3 = 0.0025 \qquad G_2 = 0.0031$ $G_4 = G_7 = 0.0042 \qquad G_5 = G_6 = 0.0045$	0.0256
VIIc	$G_1 = G_3 = G_4 = G_6 = 0.0043 \qquad G_2 = G_5 = 0.0024 \qquad G_7 = 0.0032$	0.0253
VIII	$G_1 = G_3 = G_5 = G_7 = 0.0022 \qquad G_2 = G_4 = G_6 = G_8 = 0.0032$	0.0214
IXa	$G_1 = G_4 = 0.0014 \qquad G_2 = G_3 = 0.0018$ $G_5 = G_8 = 0.0022 \qquad G_6 = G_7 = 0.0034 \qquad G_9 = 0.0026$	0.0201
IXb	$G_1 = G_2 = G_3 = G_4 = G_5 = G_6 = G_7 = G_8 = G_9 = 0.0021$	0.0185

To determine how the equilibrium configurations change as L is varied, we use the method of numerical continuation. Various software packages exist for numerical continuation of differential equations and maps, such as AUTO [13] and MatCont [10]. These packages use the method of pseudoarclength continuation in a predictor-corrector manner which enables both stable and unstable solutions to be found [11, 12]. A predicted solution is extrapolated from one or more known solutions and then corrected, using a nonlinear solver, to be a solution of the dynamical system with constraints provided by the pseudoarclength conditions. The sequence of corrected solutions that is produced can be viewed as a discretized solution branch in the appropriate system parameters. Bifurcations, detected using suitable test functions, and the corresponding bifurcating solution branches can also be continued.

We continue equilibrium configurations of the evolution equations (2.3) using the authors' own software package written entirely in MATLAB to enable the built-in `voronoi` and `voronoin` commands to be used. This package, built around MATLAB's nonlinear solver (`fsolve`), uses the same numerical algorithms as described above for AUTO and MatCont. Bifurcation detection is performed by monitoring the eigenvalues of the linearized evolution equations directly. The linearized equations are generated from (2.3) using numerical central differences.

As a measure of an equilibrium configuration in our bifurcation diagrams, we use

$$(5.1) \qquad S = \sum_{i=1}^{N} \left[(x_i - \bar{x})^2 + (y_i - \bar{y})^2 \right],$$
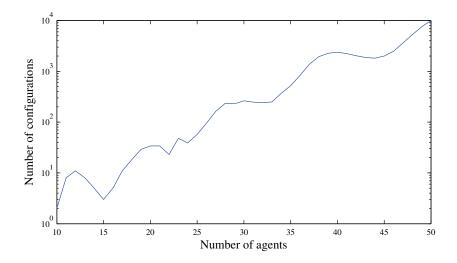
Figure 6. *Number of stable configurations as a function of the number of agents N for a square domain. Only one configuration from each group orbit of possible configurations is counted.*
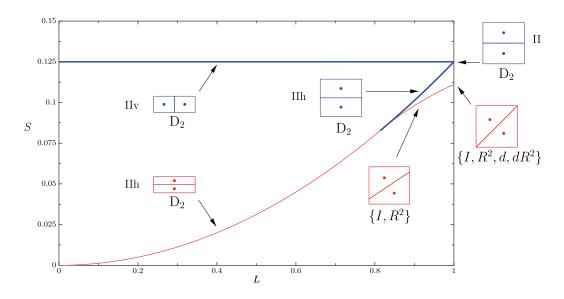

Figure 7. *Bifurcation diagram showing equilibrium configurations for $N = 2$ agents. In this and other bifurcation diagrams, thick blue (resp., thin red) lines/plots represent stable (resp., unstable) equilibrium configurations. Sample configurations are shown along with their isotropy subgroups.*

where $(\bar{x}, \bar{y})$ is the center of the domain D. Equilibrium configurations on the same group orbit have identical values of S, while solutions which are not related by symmetry typically have different values of S.

The possible bifurcations that occur are saddle-node bifurcations, in which two equilibrium configurations "collide" and disappear, and pitchfork bifurcations, which give birth to a new branch of symmetry-related equilibria with one of the Z_2 symmetries broken, for example, $D_4 \to Z_2$ or $Z_2 \to \{I\}$.

The bifurcation diagram showing equilibrium configurations for $N = 2$ agents is shown in Figure 7. For small values of L, the configuration with a vertical shared boundary for the Voronoi cells (we call this IIv) is stable, while the configuration with a horizontal shared boundary (we call this IIh) is unstable. Both IIv and IIh have D_2 symmetry. At $L = 0.817$, IIh undergoes a pitchfork bifurcation, becoming stable for larger values of L and giving birth to a new branch of unstable solutions with isotropy subgroup $\{I, R^2\} \cong Z_2$. Consequently, the solutions IIv and IIh are both stable for $0.817 \leq L \leq 1$. At $L = 1$, IIv and IIh are stable, symmetry-related solutions for the square domain (see Figure 3). At $L = 1$, the unstable configuration acquires the additional reflection symmetries d and dR^2. These arise because $L = 1$ is a degenerate case for a rectangular domain; in particular, this additional symmetry is not associated with a bifurcation. We remark that the results for $L = 1$ are consistent with [15].

An analytical treatment of the stability properties of the IIh and IIv solutions is given in the appendix.

The bifurcation diagram showing equilibrium configurations for $N = 3$ agents is shown in Figure 8. There are four different pitchfork bifurcations, described in the following for increasing L.

- $L = 0.469$: A configuration with isotropy subgroup $\{I, dR\} \cong Z_2$ gains stability, and a branch of unstable configurations with trivial isotropy subgroup $\{I\}$ is born.
- $L = 0.627$: A configuration with isotropy subgroup $\{I, dR^3\} \cong Z_2$ loses stability, and the branch of unstable configurations with trivial isotropy subgroup $\{I\}$ ceases to exist.
- $L = 0.666$: A configuration with isotropy subgroup D_2 loses stability, and a branch of unstable configurations with isotropy subgroup $\{I, dR^3\} \cong Z_2$ ceases to exist.
- $L = 0.931$: A configuration with isotropy subgroup $\{I, dR^3\}$ gains stability, and a branch of unstable configurations with trivial isotropy subgroup $\{I\}$ is born.

There is also a saddle-node bifurcation at $L = 0.607$ involving solutions with isotropy subgroup $\{I, dR^3\} \cong Z_2$. Details of these bifurcations can be seen in Figures 9 and 10. Note that the unstable solutions with trivial isotropy subgroup $\{I\}$ which are born in the pitchfork bifurcation at $L = 0.931$ acquire the additional reflection symmetry d at $L = 1$; this arises from the degeneracy of the domain shape at $L = 1$. We see that several ranges of L values exist for which there are stable equilibria which are not related by symmetry.

The bifurcation diagrams showing equilibrium configurations for $N = 4$ and $N = 5$ agents are shown in Figures 11, 12, and 13. Because of the complexity of these diagrams, we do not describe them in detail, nor do we specify the isotropy subgroups of the various equilibrium configurations. But we do note that there are ranges of L for which there are stable equilibria which are not related by symmetry.

6. Experiments with robots. As a verification of the relevance of the theoretical and numerical results described above for a real system, we have conducted territorial experiments using three-wheeled inverted pendulum robots. In these experiments, an MTV-7310 camera mounted above the robots with a resolution of 470×570 is used to detect robot positions and orientations. The video signals are available in real time via a frame grabber board PicPort-Stereo-HrD and image processing software HALCON. The sampling period of the controller
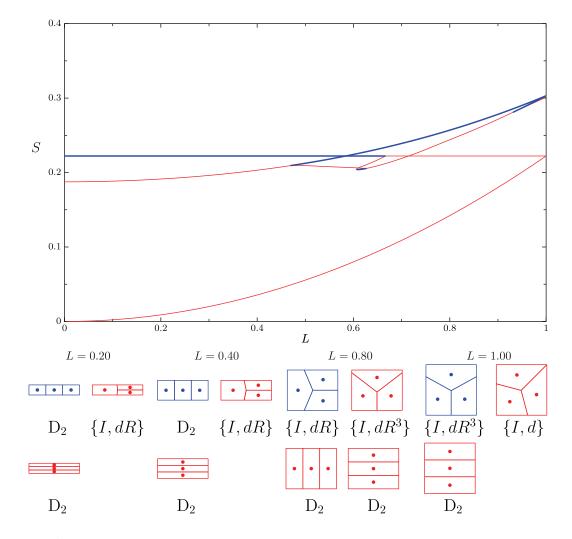
Figure 8. *Bifurcation diagram showing equilibrium configurations for N = 3 agents. For the specified values of L, the plots of the configurations are shown for decreasing S value, in the following order: First row first column, first row second column, second row first column, etc. The isotropy subgroups of these configurations are indicated. More detail is shown in Figures 9 and 10.*

and the frame rate provided by the camera are 0.33 ms and 30 fps, respectively. The position and orientation of the robots are calculated by using image processing. Based on this information, the PC computes the velocity control input and sends it to each robot via the embedded wireless communication device Wiport (LANTRONIX). The Wiport attached to each robot receives the signal and sends it to the microcomputer via serial communications. Figure 14 illustrates the information flow chart including the robots, camera, and PC, respectively. Note that we employ the coverage control scheme for unicycle models presented in [9] since these robots have mobile wheeled dynamics. (We remark that that this algorithm is not exactly implemented due to delays in sensing, processing, and actuation.) The equilibrium configurations will be the same for this model as those described above for the model from [36].
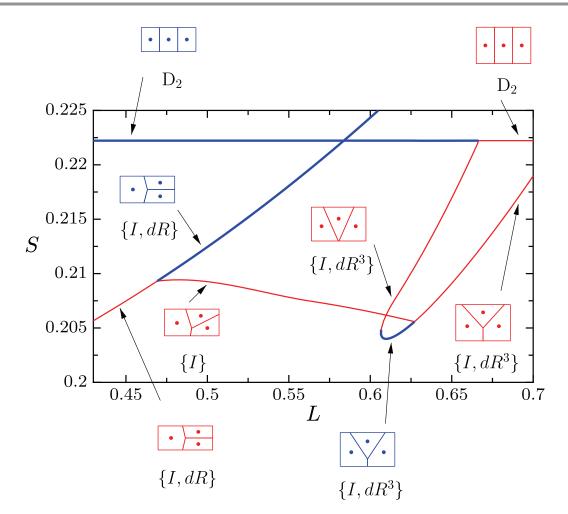
Figure 9. *Details of the bifurcation diagram shown in Figure* 8.

The experiment shown in Figure 15(a) sweeps the L value for the domain very slowly from $L = 0.74$ to $L = 0.30$. (In practice, this is accomplished by dynamically adjusting the anisotropy of the Voronoi calculation for all agents [20, 21].) We see that at approximately $L = 0.30$ the system switches from a configuration with one type of symmetry to a configuration with a different one. Similarly, Figure 15(b) shows results from an experiment in which L is swept from $L = 0.30$ to $L = 0.74$, where again the system switches from a configuration with one type of symmetry to a configuration with a different one. These results are consistent with the bifurcation diagram shown in Figure 8, although the transitions occur at values of L beyond those for which one state loses stability; this is due to the fact that the sweeps in L occur at finite, rather than infinitesimal, speed. Transitions between different equilibrium configurations closer to the relevant bifurcations are shown in Figure 16.

7. Conclusion. We have analyzed the territorial model from [36], which is based on Voronoi tessellations to account for interactions between individuals in determining territo-
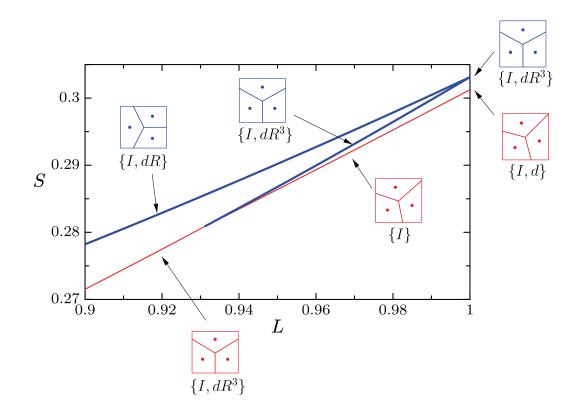
Figure 10. *Details of the bifurcation diagram shown in Figure* 8.

ries. For rectangular domains and for small population sizes, we found that there are distinct coexisting stable equilibrium configurations, including the possibility of stable equilibria that are *not* related by symmetry to each other and which represent truly distinct configurations that the population can end up in. The configuration that the population equilibrates to, and the cell in which each agent ends up, is determined by the initial positions of the agents. By considering initial positions distributed randomly on the square, we gave a statistical characterization of the likelihood of the system reaching these equilibria; this can be interpreted as a statistical characterization of the relative sizes of different basins of attraction for the equilibria. Furthermore, we found that the final territory that an agent obtains can have a wide range of areas, which suggests that an individual can obtain a competitive advantage or disadvantage due entirely to the initial positions of the agents. By treating the ratio of the length of the shorter side to the length of the longer side of the rectangle as a bifurcation parameter, we numerically explored how stable and unstable equilibrium configurations are related to each other. Finally, we verified our numerical results for three agents through experiments using robots which move according to a related territorial algorithm.

Although the geometry considered here is too special to be of direct relevance to field observations, our results suggest how controlled laboratory experimentation could be used to verify or discount this particular model of territorial behavior for different species. One simply randomly positions a small number of individuals in a square or rectangular domain
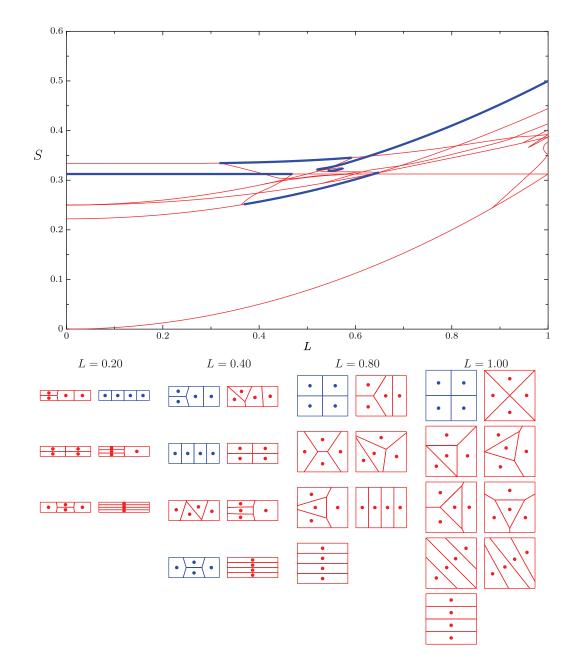
Figure 11. *Bifurcation diagram showing equilibrium configurations for $N = 4$ agents. For the specified values of L, the plots of the configurations are shown for decreasing values of S, in the order explained in the caption of Figure* 8.
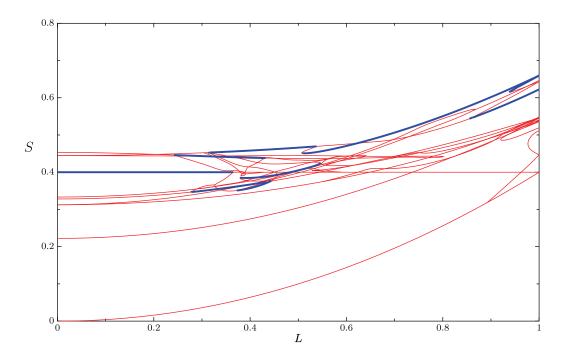
Figure 12. *Bifurcation diagram showing equilibrium configurations for $N = 5$ agents. Corresponding equilibrium configurations are shown in Figure 13.*

and observes over multiple trials what configuration they settle down in. If the agents are effectively using the model from [36] to determine their territories, then, depending on the number of agents and the shape of the container, on some trials one would expect settling to a particular equilibrium of one type, and in others settling to an equilibrium of another nonsymmetry-related type.

Coexisting stable equilibrium configurations can be present for more general domains, as illustrated in Figure 17. Visually, these equilibria resemble particular equilibria found for "nearby" rectangular domains. A more detailed study of equilibria for nonrectangular domains is outside the scope of the present study.

The presence of coexisting stable equilibria also suggests that noise-induced transitions between different states might occur. Such transitions have recently been identified for biological systems for the switching between symmetry-related clockwise and counterclockwise motions for marching locusts constrained to a ring [6], and switching between qualitatively different collective motion states [27].

Appendix. We consider the stability of the IIh equilibrium configuration for $N = 2$. We let $\mathbf{x}_i = (x_i, y_i)$ and $\mathbf{c}_i = (c_{ix}, c_{iy})$, giving

(A.1)
$$x_i^{(n+1)} = x_i^{(n)} + \left(c_{ix}^{(n)} - x_i^{(n)}\right)/M \equiv f_{ix}(x_1^{(n)}, y_1^{(n)}, x_2^{(n)}, y_2^{(n)}),$$

(A.2)
$$y_i^{(n+1)} = y_i^{(n)} + \left(c_{iy}^{(n)} - y_i^{(n)}\right)/M \equiv f_{iy}(x_1^{(n)}, y_1^{(n)}, x_2^{(n)}, y_2^{(n)}),$$
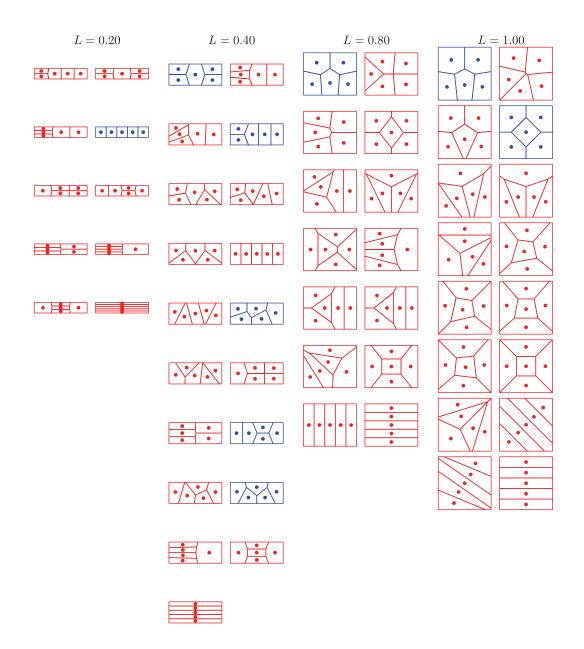
Figure 13. *Equilibrium configurations for $N = 5$ agents. For the specified values of L, the plots of the configurations are shown for decreasing values of S according to Figure 12, in the order explained in the caption of Figure 8.*
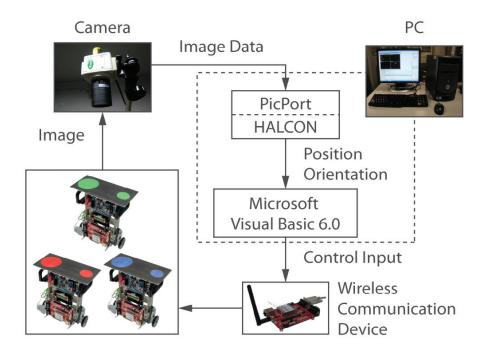
Figure 14. *Information flow for robots, camera, and PC. This setup allows robots to divide territory using Voronoi-based algorithms.*

where $i = 1, 2$. For convenience, we choose the domain to be the set

$$D = \left\{ (x, y) \mid -\frac{1}{2} \le x \le \frac{1}{2}, -\frac{L}{2} \le y \le \frac{L}{2} \right\},$$

so that the IIh equilibrium configuration corresponds to

(A.3) $$(x_1, y_1) = (0, L/4), \qquad (x_2, y_2) = (0, -L/4).$$

For general positions for the agents, it is readily shown that the line

$$y_b(x) = \frac{x_2 - x_1}{y_1 - y_2} \left(x - \frac{1}{2}(x_1 + x_2) \right) + \frac{1}{2}(y_1 + y_2)$$

forms the boundary between the Voronoi cells. Assuming that the system is close to the IIh equilibrium, this line will intersect the domain boundary at $x = \pm 1/2$. We can thus calculate
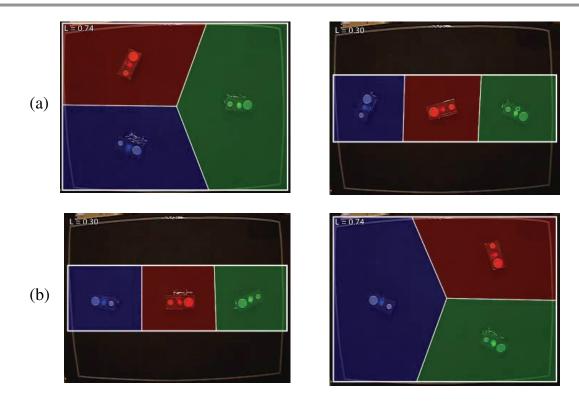
Figure 15. *Experiments in which L is slowly swept* (a) *from L = 0.74 to L = 0.30 and* (b) *from L = 0.30 to L = 0.74 showing (left) initial states and (right) final states. See the associated movie files* (71012_04.mpg [10.3MB] *and* 71012_05.mpg [12.8MB]). *Note that the occasional flickering in the movies corresponds to brief times for which the camera fails to identify one of the robots; this happens so quickly that the effect on the dynamics of the robots is negligible.*

the centroids of the Voronoi cells from the following formulas:

$$c_{1x} = \frac{1}{|V_1|} \int_{V_1} x \, dx \, dy = \frac{1}{|V_1|} \int_{-1/2}^{1/2} x \, dx \int_{y_b(x)}^{L/2} dy,$$

$$c_{1y} = \frac{1}{|V_1|} \int_{V_1} y \, dx \, dy = \frac{1}{|V_1|} \int_{-1/2}^{1/2} dx \int_{y_b(x)}^{L/2} y \, dy,$$

$$c_{2x} = \frac{1}{|V_2|} \int_{V_2} x \, dx \, dy = \frac{1}{|V_2|} \int_{-1/2}^{1/2} x \, dx \int_{-L/2}^{y_b(x)} dy,$$

$$c_{2y} = \frac{1}{|V_2|} \int_{V_2} y \, dx \, dy = \frac{1}{|V_2|} \int_{-1/2}^{1/2} dx \int_{-L/2}^{y_b(x)} y \, dy,$$

where

$$|V_1| = \int_{-1/2}^{1/2} dx \int_{y_b(x)}^{L/2} dy, \qquad |V_2| = \int_{-1/2}^{1/2} dx \int_{-L/2}^{y_b(x)} dy.$$

After solving these integrals to obtain the centroids as a function of x_1, y_1, x_2, y_2, the Jacobian
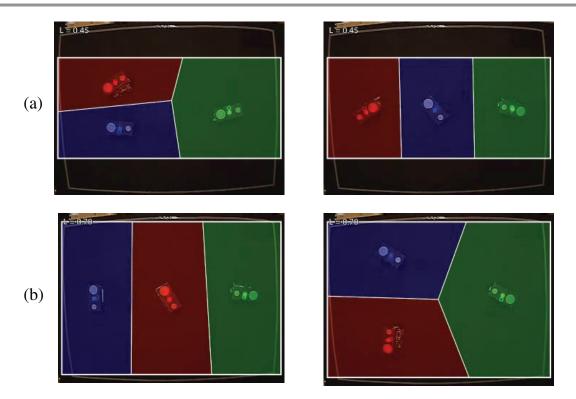
Figure 16. *Experiments for* (a) $L = 0.45$ *and* (b) $L = 0.70$ *for which the system transitions from (left) an unstable equilibrium configuration to (right) a stable one. See the associated movie files (71012_06.mpg [8.7MB] and 71012_07.mpg [13.2MB]). The occasional flickering in the movies does not affect the dynamics of the robots, as described in the caption of Figure* 15.

matrix of (A.1), (A.2) evaluated at the IIh equilibrium (A.3) is found to be

$$
J = \begin{pmatrix}
\frac{\partial f_{1x}}{\partial x_1} & \frac{\partial f_{1x}}{\partial y_1} & \frac{\partial f_{1x}}{\partial x_2} & \frac{\partial f_{1x}}{\partial y_2} \\[2mm]
\frac{\partial f_{1y}}{\partial x_1} & \frac{\partial f_{1y}}{\partial y_1} & \frac{\partial f_{1y}}{\partial x_2} & \frac{\partial f_{1y}}{\partial y_2} \\[2mm]
\frac{\partial f_{2x}}{\partial x_1} & \frac{\partial f_{2x}}{\partial y_1} & \frac{\partial f_{2x}}{\partial x_2} & \frac{\partial f_{2x}}{\partial y_2} \\[2mm]
\frac{\partial f_{2y}}{\partial x_1} & \frac{\partial f_{2y}}{\partial y_1} & \frac{\partial f_{2y}}{\partial x_2} & \frac{\partial f_{2y}}{\partial y_2}
\end{pmatrix}
$$

$$
= \begin{pmatrix}
1 - \frac{1}{M} + \frac{1}{3L^2 M} & 0 & -\frac{1}{3L^2 M} & 0 \\[2mm]
0 & 1 - \frac{3}{4M} & 0 & \frac{1}{4M} \\[2mm]
-\frac{1}{3L^2 M} & 0 & 1 - \frac{1}{M} + \frac{1}{3L^2 M} & 0 \\[2mm]
0 & \frac{1}{4M} & 0 & 1 - \frac{3}{4M}
\end{pmatrix} .
$$

Since $|V_1| = |V_2|$ at the equilibrium, the Jacobian is symmetric, and therefore its eigenvalues must be real, as expected from the discussion in the main text. The eigenvalues are

(A.4) $\qquad 1 - \dfrac{1}{M}, \qquad 1 - \dfrac{1}{M}, \qquad 1 - \dfrac{1}{2M}, \qquad 1 + \dfrac{\frac{2}{3L^2} - 1}{M} \equiv E(L; M).$
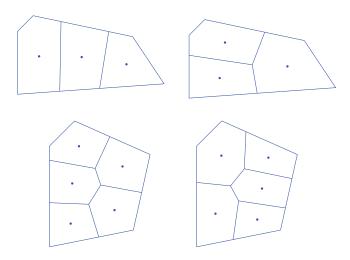
Figure 17. *Coexisting stable equilibrium configurations for nonrectangular domains for (top) $N = 3$ and (bottom) $N = 5$ agents.*

We note that the eigenvalues take the form expected from the proof of Proposition 3.2. The first three eigenvalues always lie within the unit circle for $M \geq 1$. The last eigenvalue is inside the unit circle for $L > \sqrt{2/3}$ and outside for $L < \sqrt{2/3}$. Treating L as a bifurcation parameter, we conclude that a steady bifurcation occurs at $L = \sqrt{2/3} \approx 0.8165$, which is confirmed by the numerical result shown in Figure 7.

A similar calculation can be done to deduce the eigenvalues of the Jacobian of the IIv solution. However, we can more easily show that it is always stable by recognizing that the above calculation also holds for $L > 1$, but then the equilibrium (A.3), upon rotation of the domain by 90° and rescaling length, corresponds to the IIv equilibrium for $L < 1$. The first three eigenvalues in (A.4) will clearly always lie within the unit circle for $M \geq 1$. Furthermore, recognizing that

$$0 < E(1; M) = 1 - \frac{1}{3M} < 1, \qquad \frac{\partial E(L; M)}{\partial L} = -\frac{4}{3L^2 M} < 0,$$

$$0 < \lim_{L \to \infty} E(L; M) = 1 - \frac{1}{M} < 1,$$

we conclude that the fourth eigenvalue must also always lie within the unit circle. Thus, the IIh solution is stable for all $L > 1$, so that the IIv solution is stable for all $L < 1$.

In principle, similar analytical arguments can be used to study the stability properties of equilibrium configurations for different numbers of agents N. This would be straightforward but tedious in practice.

REFERENCES

[1] E. S. ADAMS, *Approaches to the study of territory size and shape*, Ann. Rev. Ecol. Syst., 32 (2001), pp. 277–303.

[2] G. W. BARLOW *Hexagonal territories*, Anim. Behav., 22 (1974), pp. 876–878.

[3] P. A. BUCKLEY AND F. G. BUCKLEY, *Hexagonal packing of Royal Tern nests*, Auk., 94 (1977), pp. 36–43.

[4] D. A. CLAYTON AND T. C. VAUGHAN, *Pentagonal territories of the mudskipper, Boleophthalmus boddarti (Pisces: Gobiidae)*, Copeia, 1 (1982), pp. 233–235.

[5] D. A. CLAYTON AND J. M. WRIGHT, *Mud-walled territories and feeding behaviour of Boleophthalmus boddarti (Pisces: Gobiidae) on the mudflats of Kuwait*, J. Ethol., 7 (1989), pp. 91–95.

[6] J. BUHL, D. J. T. SUMPTER, I. D. COUZIN, J. J. HALE, E. DESPLAND, E. R. MILLER, AND S. J. SIMPSON, *From disorder to order in marching locusts*, Science, 312 (2006), pp. 1402–1406.

[7] J. BURKHARDT, http://www.scs.fsu.edu/~burkardt/m_src/geometry/geometry.html, 2009.

[8] P. CHOSSAT AND R. LAUTERBACH, *Methods in Equivariant Bifurcations and Dynamical Systems*, World Scientific, Singapore, 2000.

[9] J. CORTÉS, S. MARTÍNEZ, T. KARATAS, AND F. BULLO, *Coverage control for mobile sensing networks*, IEEE Trans. Robotics and Automation, 20 (2004), pp. 243–255.

[10] A. DHOOGE, W. GOVAERTS, Y. A. KUZNETSOV, W. MESTROM, A. M. RIET, AND B. SAUTOIS, *MAT-CONT and CL_MATCONT: Continuation toolboxes in MATLAB*, http://www.matcont.ugent.be/, 2005.

[11] E. J. DOEDEL, H. B. KELLER, AND J. P. KERNEVEZ, *Numerical analysis and control of bifurcation problems*, I, Internat. J. Bifur. Chaos Appl. Sci. Engrg., 1 (1991), pp. 493–520.

[12] E. J. DOEDEL, H. B. KELLER, AND J. P. KERNEVEZ, *Numerical analysis and control of bifurcation problems*, II, Internat. J. Bifur. Chaos Appl. Sci. Engrg., 1 (1991), pp. 745–772.

[13] E. J. DOEDEL, A. R. CHAMPNEYS, T. F. FAIRGRIEVE, Y. A. KUZNETSOV, B. SANDSTEDE, AND X. WANG, *AUTO 97: Continuation and Bifurcation Software for Ordinary Differential Equations*, http://indy.cs.concordia.ca/auto/, 1998.

[14] C. P. DONCASTER AND R. WOODROFFE, *Den site can determine shape and size of badger territories: Implications for group-living*, Oikos, 66 (1993), pp. 88–93.

[15] Q. DU, V. FABER, AND M. GUNZBURGER, *Centroidal Voronoi tessellations: Applications and algorithms*, SIAM Rev., 41 (1999), pp. 637–676.

[16] Q. DU, M. EMELIANENKO, AND L. JU, *Convergence of the Lloyd algorithm for computing centroidal Voronoi tessellations*, SIAM J. Numer. Anal., 44 (2006), pp. 102–119.

[17] M. GOLUBITSKY, I. STEWART, AND D. G. SCHAEFFER, *Singularities and Groups in Bifurcation Theory*, Vol. 2, Springer, New York, 1988.

[18] M. GOLUBITSKY AND I. STEWART, *The Symmetry Perspective*, Birkhäuser, Basel, 2002.

[19] P. R. GRANT, *Polyhedral territories of animals*, Amer. Naturalist, 102 (1968), pp. 75–80.

[20] A. GUSRIALDI, S. HIRCHE, T. HATANAKA, AND M. FUJITA, *Voronoi based coverage control with anisotropic sensors*, in Proceedings of the 2008 American Control Conference, 2008, pp. 736–741.

[21] A. GUSRIALDI, S. HIRCHE, D. ASIKIN, T. HATANAKA, AND M. FUJITA, *Voronoi based coverage control with anisotropic sensors and experimental case study*, Intelligent Service Robotics, to appear, 2009.

[22] M. HASEGAWA AND M. TANEMURA, *On the pattern of space division by territories*, Ann. Inst. Statist. Math., 28 (1976), pp. 509–519.

[23] M. HASEGAWA AND M. TANEMURA, *Spatial patterns of territories*, in Recent Developments in Statistical Inference and Data Analysis, K. Matusita, ed., North–Holland, Amsterdam, 1980, pp. 73–78.

[24] H. HONDA, *Description of cellular patterns by Dirichlet domains: The two-dimensional case*, J. Theoret. Biol., 72 (1978), pp. 523–543.

[25] R. B. HOYLE, *Pattern Formation: An Introduction to Methods*, Cambridge University Press, Cambridge, UK, 2006.

[26] C. H. HSIEH, Y.-L. CHUANG, Y. HUANG, K. K. LEUNG, A. L. BERTOZZI, AND E. FRAZZOLI, *An economical micro-car testbed for validation of cooperative control strategies*, in Proceedings of the 2006 American Control Conference, Minneapolis, MN, 2006, pp. 1446–1451.

[27] A. KOLPAS, J. MOEHLIS, AND I. G. KEVREKIDIS, *Stochasticity-induced switching between collective motion states*, in Proc. Natl. Acad. Sci. USA, 104 (2007), pp. 5931–5935.

[28] M. A. Lewis and J. D. Murray, *Modeling territoriality and wolf deer interactions*, Nature, 366 (1993), pp. 738–740.

[29] J. S. Lomont, *Applications of Finite Groups*, Dover, New York, 1993.

[30] J. Maynard Smith, *Evolution and the Theory of Games*, Cambridge University Press, Cambridge, UK, 1982.

[31] J. Moehlis and E. Knobloch, *Equivariant dynamical systems*, available online from http://www.scholarpedia.org/article/Equivariant_Dynamical_Systems, 2007.

[32] P. R. Moorcroft and M. A. Lewis, *Mechanistic Home Range Analysis*, Princeton University Press, Princeton, 2006.

[33] L. J. Morrell and H. Kokko, *Bridging the gap between mechanistic and adaptive explanations of territory formation*, Behav. Ecol. Sociobiol., 57 (2005), pp. 381–390.

[34] H. M. Pereira, A. Bergman, and J. Roughgarden, *Socially stable territories: The negotiation of space by interacting foragers*, Amer. Natur., 161 (2003), pp. 143–152.

[35] J. A. Stampls and V. V. Krishnan, *A learning-based model of territory establishment*, Q. Rev. Biol., 74 (1999), pp. 291–318.

[36] M. Tanemura and M. Hasegawa, *Geometrical models of territory.* I. *Models for synchronous and asynchronous settlement of territories*, J. Theoret. Biol., 82 (1980), pp. 477–496.

[37] E. O. Wilson, *Sociobiology: The New Synthesis*, Harvard University Press, Cambridge, MA, 1975.